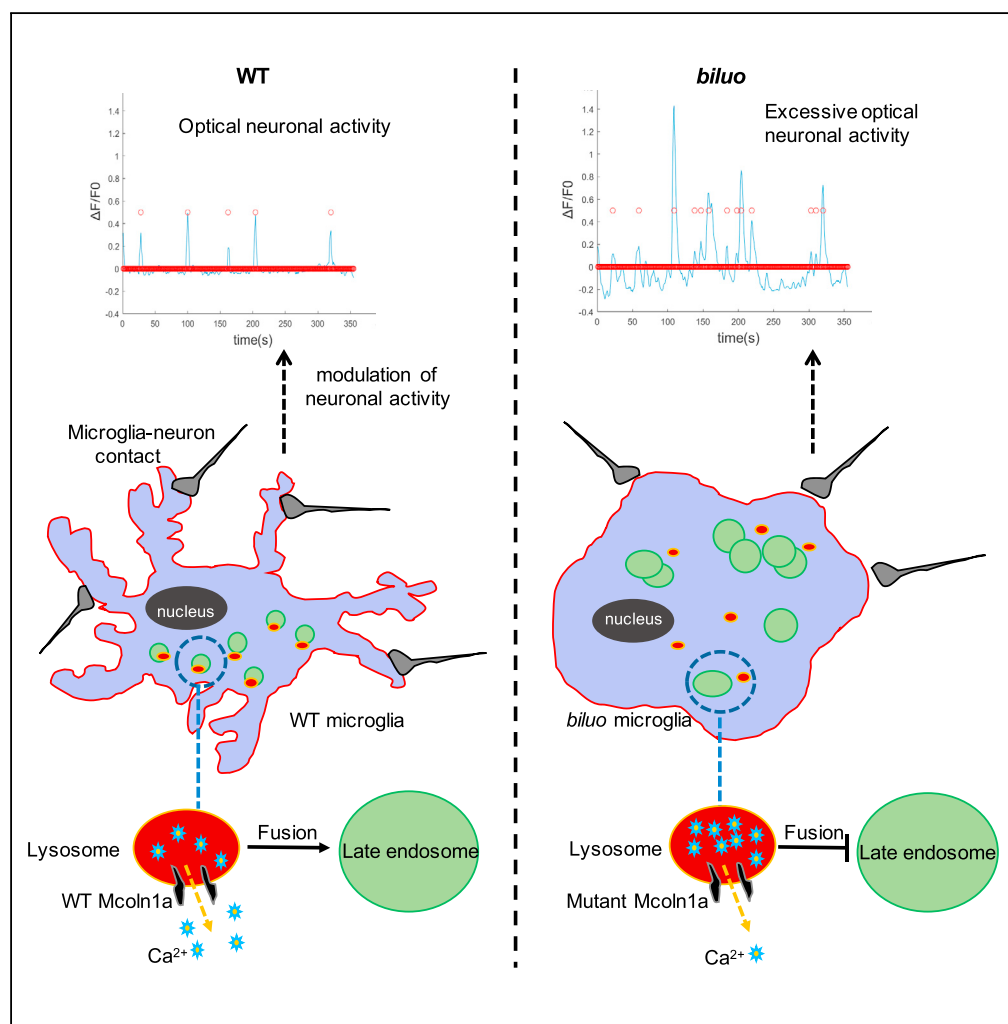


Article

Dysregulation of Microglial Function Contributes to Neuronal Impairment in *Mcoln1a*-Deficient Zebrafish



Wan Jin, Yimei Dai, Funing Li, ..., Jiulin Du, Wenqing Zhang, Zilong Wen

mczhangwq@scut.edu.cn
(W.Z.)
zilong@ust.hk (Z.W.)

HIGHLIGHTS

mcoln1a-deficient fish display microglia impairment and aberrant neuronal activity

The aberrant neuronal activity can be rescued by expressing WT *mcoln1a* in microglia

Impairment of microglia-neuron contact contributes to the aberrant neuronal activity

Jin et al., iScience 13, 391–401
March 29, 2019 © 2019 The Author(s).
<https://doi.org/10.1016/j.isci.2019.02.031>



Article

Dysregulation of Microglial Function Contributes to Neuronal Impairment in *Mcoln1a*-Deficient Zebrafish

Wan Jin,^{1,5} Yimei Dai,^{1,5} Funing Li,² Lu Zhu,¹ Zhibin Huang,³ Wei Liu,³ Jianchao Li,¹ Mingjie Zhang,¹ Jiulin Du,² Wenqing Zhang,^{3,*} and Zilong Wen^{1,4,6,*}

SUMMARY

Type IV mucolipidosis (ML-IV) is a neurodegenerative lysosome storage disorder caused by mutations in the *MCOLN1* gene. However, the cellular and molecular bases underlying the neuronal phenotypes of ML-IV disease remain elusive. Using a forward genetic screening, we identified a zebrafish mutant, *biluo*, that harbors a hypomorphic mutation in *mcoln1a*, one of the two zebrafish homologs of mammalian *MCOLN1*. The *mcoln1a*-deficient mutants display phenotypes partially recapitulating the key features of ML-IV disorder, including the accumulation of enlarged late endosomes in microglia and aberrant neuronal activities in both spontaneous and visual-evoking conditions in optic tectal neurons. We further show that the accumulation of enlarged late endosomes in microglia is caused by the impairment of late endosome and lysosome fusion and the aberrant neuronal activities can be partially rescued by the reconstitution of *Mcoln1a* function in microglia. Our findings suggest that dysregulation of microglial function may contribute to the development and progression of ML-IV disease.

INTRODUCTION

Microglia are the resident macrophages in the central nervous system (CNS) (Hanisch and Kettenmann, 2007; Kim and de Vellis, 2005). They were initially characterized by Spanish neuroscientist del Rio Hortega in 1919 as a population of cells in the brain distinct from neurons, oligodendrocytes, and astrocytes (Hortega, 1919). For years, it has been thought that microglia predominately act as immune cells to remove cellular debris and infectious agents in the CNS (Kreutzberg, 1995; Napoli and Neumann, 2009). But recent studies have revealed that, in addition to functioning as immune response, microglia also play critical roles in the regulation of neural development and functions (Bialas and Stevens, 2013; Li et al., 2012b; Paolicelli et al., 2011; Schafer et al., 2012; Squarzoni et al., 2014; Tremblay et al., 2010; Wake et al., 2009). More importantly, aberrant microglia activities have been found to be closely associated with a number of neurodegenerative disorders, including Multiple Sclerosis, Autism, and Alzheimer and Parkinson diseases (Chastain et al., 2011; Davoust et al., 2008; Derecki et al., 2012; Graeber and Streit, 2010; Iaccarino et al., 2016; Kim and de Vellis, 2005; Ponomarev et al., 2005). Although the precise underlying mechanism remains unclear, it is generally believed that pathological stimuli such as amyloid β plaques can trigger the activation of microglia to release pro-inflammatory and neurotoxic factors, which can cause neuronal cell death and neural circuit impairment (Block et al., 2007; Kim et al., 2015; Qin et al., 2004; Takeuchi et al., 2006; Thompson and Tsirka, 2017). On the other hand, several studies have indicated that microglia play a beneficial role during the onset and the progression of Alzheimer disease by removing the amyloid β plaques accumulated in the CNS (Herz et al., 2017; Hickman et al., 2008). Thus, a comprehensive understanding of the precise roles of microglia in different neurodegenerative disorders may provide therapeutic treatment for these disorders.

Type IV mucolipidosis (ML-IV) is a neurodegenerative and lysosomal storage disorder with various neuronal symptoms, including psychomotor retardation, hypotonia, corneal opacities, and retinal degeneration (Bargal et al., 2000; Bassi et al., 2000; Wakabayashi et al., 2011). Patients with severe ML-IV display failure of sitting, crawling, and standing within infancy as well as are non-verbal and blind during the teenage stage (Folkert et al., 1995). Genetically, ML-IV disorder is caused by mutations in transient receptor potential cation channel, mucolipin 1 (*MCOLN1*), a cation-permeable channel predominantly expressing on the membrane of late endosomes and lysosomes (LELs) (Bach, 2005; Manzoni et al., 2004). It is known that *MCOLN1* channel releasing ions from the lumen of LELs to cytosol in response to different stimuli and

¹Division of Life Science, State Key Laboratory of Molecular Neuroscience and Center of Systems Biology and Human Health, the Hong Kong University of Science and Technology, Clear Water Bay, Kowloon, Hong Kong, PR. China

²Institute of Neuroscience, State Key Laboratory of Neuroscience, CAS Center for Excellence in Brain Science and Intelligence Technology, Chinese Academy of Sciences, 320 Yue-Yang Road, Shanghai 200031, PR. China

³Department of Cell, Developmental and Integrative Biology, School of Medicine, South China University of Technology, Guangzhou 510006, PR. China

⁴Shenzhen Key Laboratory for Neuronal Structural Biology, Biomedical Research Institute, Shenzhen Peking University–Hong Kong University of Science and Technology Medical Center, Shenzhen 518036, PR. China

⁵These authors contributed equally

⁶Lead Contact

*Correspondence:
mczhangwq@scut.edu.cn
(W.Z.), zilong@ust.hk (Z.W.)

<https://doi.org/10.1016/j.isci.2019.02.031>



the MCOLN1-mediated Ca^{2+} efflux are critical for endosomal acidification and organelle homeostasis (Dong et al., 2008, 2009, 2010; LaPlante et al., 2002, 2004; Luzio et al., 2007; Morgan et al., 2011). Studies in animal models have revealed that excessive neuronal cell death and muscle dystrophy contribute to the development of ML-IV disorder (Li et al., 2017; Venkatachalam et al., 2008). Intriguingly, histological staining of human brains of patients with ML-IV has revealed that both neurons and microglia display abnormal morphology such as the accumulation of membrane-bounded storage bodies in cytoplasm (Folkert et al., 1995), indicating that both neurons and microglia contribute to the development of the disease. This notion is further supported by the studies in *MCOLN1*-deficient mice and drosophila, showing that transplantation of wild-type (WT) bone marrow cells into *MCOLN1*-deficient mice and reconstitution of WT *MCOLN1* in hemocytes in *mcoln1*-deficient drosophila can rescue, at least in part, the motor deficiency (Walker and Montell, 2016; Venkatachalam et al., 2008). However, since drosophila lacks microglia and bone marrow cell transplantation in mice has a relatively low efficiency of microglia reconstitution, whether microglia contribute to the development of ML-IV disorder and the underlying mechanism remain to be clarified.

Zebrafish has recently emerged as an alternative vertebrate model system for the study of microglia development and homeostasis (Casano and Peri, 2015). Because of its small size and transparency, zebrafish provides a platform to perform unbiased large-scale forward genetic screening and *in vivo* time-lapse imaging analysis (Driever et al., 1996; Haffter et al., 1996). The development and function of microglia appear to be evolutionarily conserved between zebrafish and mammals (Casano and Peri, 2015). In zebrafish, microglia begin to populate the brain from 2.5 days post fertilization (dpf) (Herbomel et al., 1999, 2001). This early population of microglial precursors originates from the rostral blood island (Xu et al., 2015), and they are promoted to colonize the developing zebrafish brain by the signals released from the apoptotic neurons, which occurs naturally during neurogenesis (Xu et al., 2016; Casano et al., 2016) and by the IL34-Csf1r signaling pathway (Wu et al., 2018). Similar to mammalian microglia, zebrafish microglia are capable of removing cellular debris in the CNS and are actively involved in neural activity (Li et al., 2012b; Peri and Nusslein-Volhard, 2008). A recent study has shown that zebrafish consists of two orthologs, *mcoln1a* and *mcoln1b*, of *MCOLN1*, and *mcoln1ab* double-mutant zebrafish display retinal and neuromuscular defects similar to the patients with ML-IV with *MCOLN1* deficiency (Folkert et al., 1995; Li et al., 2017; Wakabayashi et al., 2011). Thus, zebrafish appears to be a suitable model for studying the role of microglia in the pathogenesis of ML-IV disorder.

Here, we report the isolation and characterization of a zebrafish mutant *biluo*, which harbors a hypomorphic mutation in the *mcoln1a* gene, one of the two zebrafish homologs of *MCOLN1*. We found that loss of *Mcoln1a* function blocks late endosome and lysosome fusion in microglia and neurons. Moreover, *mcoln1a*-deficient zebrafish exhibit aberrant neuronal activities at early embryonic stages, which is caused at least in part by the dysregulation of microglial function.

RESULTS

biluo Mutant Microglia Display Aberrant Morphologies at Embryonic Stage

To uncover regulators involved in the development and function of microglia, we carried out an N-ethyl-N-nitrosourea-based forward genetic screening in zebrafish to search for mutants defective in microglia (Venugopal et al., 2007). Neutral red, a classical histological dye that can accumulate in lysosomes (Herbomel et al., 2001), was used as a marker to track microglia in zebrafish embryos. One mutant, *biluo*, which lacked neutral red staining in the brain but maintained normal general development (Figure 1A), was identified and selected for further in-depth study.

To further characterize the microglia phenotype in *biluo* mutants, we examined the expression of other microglia markers, including lymphocyte cytosolic plastin 1 (*Lcp1*), a myeloid marker for macrophages and their precursors (Herbomel et al., 1999; Jin et al., 2012), in *biluo* mutants. As shown in Figure 1B, anti-*Lcp1* antibody staining revealed a comparable number of *Lcp1*⁺ microglia in the brains of *biluo* mutants and siblings (Figure 1B), indicating that the lack of neutral red staining in *biluo* mutant fish is not due to the absence of microglia but rather attributed to the functional impairment of these cells. This notion was further supported by the differential interference contrast (DIC) microscopic analysis, which showed that *biluo* mutant microglia displayed an enlarged and round-shaped morphology with the accumulation of membrane-bound storage bodies in the cytoplasm (Figure 1B).

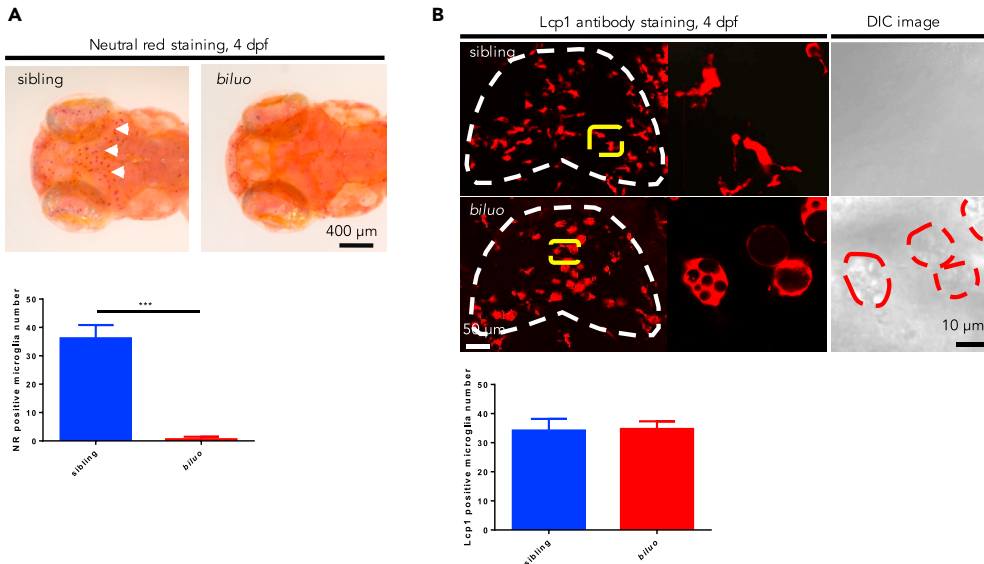


Figure 1. Aberrant Morphology of Embryonic Microglia in *biluo* Mutants

(A) Neutral red staining of 4-dpf siblings and mutants. Abundant microglia (white arrows) are positive for neutral red in the siblings (left) but not in the mutants. Quantification data of neutral red positive microglia number in 4-dpf siblings and mutants. $n(\text{Sibling}) = 7$ embryos, $n(\text{biluo}) = 6$ embryos. *** $p < 0.001$. Error bars represent mean \pm SD.

(B) Lymphocyte cytosolic Iplastin1 (Lcp1) antibody staining and DIC images of the brains of 4 dpf embryos indicate that microglia are present in *biluo* mutants but exhibit an abnormal enlarged morphology with accumulation of vacuoles. Quantification data of Lcp1 positive microglia number in 4 dpf siblings and mutants. White dashed lines indicate the optic tectum, yellow lines indicate the microglia presented in high magnification view on the right, and red dashed lines indicate the mutant microglia under DIC view. $n(\text{Sibling}) = 4$ embryos, $n(\text{biluo}) = 6$ embryos. Error bars represent mean \pm SD.

The *biluo* Gene Encodes *Mcoln1a* Protein

To identify the genetic lesion in *biluo* mutants, positional cloning was carried out. Bulk segregation analysis mapped the *biluo* mutation to chromosome 1, and subsequent fine-mapping analysis positioned the mutation on an 82-kb region containing four genes: *serhl*, *trappc5*, *mcoln1a*, and *si:Ch211-214C7.4* (Figure 2A). Sequencing of the coding regions of the four candidates revealed a point mutation in the *mcoln1a* gene, resulting in the substitution of a highly conserved Threonine (T) 519 with Isoleucine (I) (Figures 2B and 2C).

Mcoln1a is one of the two zebrafish counterparts of MCOLN1, a member of the mucolipin subfamily of transient receptor potential channels, which mediates the release of ions, such as Ca^{2+} , from the lumen of LEIs to cytosol (Dong et al., 2008, 2009; LaPlante et al., 2002, 2004; Luzio et al., 2007; Morgan et al., 2011). Previous studies have shown that multiple endocytic-related cellular processes are regulated by the Ca^{2+} released from lysosomal lumen to cytoplasm through the MCOLN1 channel (Dong et al., 2010; Luzio et al., 2007; Morgan et al., 2011). Based on recently solved Cryo-EM structure of mouse MCOLN1 (PDB: 5WPV) (Chen et al., 2017), we constructed a 3D homology model of zebrafish *Mcoln1a* and found the amino acid T519 is located in the sixth α -Helix of the transmembrane domain (Figure 2D). We therefore reasoned that the T to I mutation at residue 519 might be sufficient to disrupt the function of *Mcoln1a* channel, resulting in aberrant microglia phenotype in *biluo* mutants. To confirm this was indeed the case, we generated a *Tg(coro1a:mcoln1a)* transgenic line, in which WT *mcoln1a* is under the control of leukocyte-specific *coro1a* promoter (Li et al., 2012a). Whole-mount *in situ* hybridization and RT-PCR analysis confirmed that WT *mcoln1a* transgene was expressed specifically in myeloid precursors and microglia in *Tg(coro1a:mcoln1a)* transgenic fish (Figure S1). As anticipated, aberrant microglia phenotype was fully rescued in *biluo;Tg(coro1a:mcoln1a)* transgenic mutant fish (Figure 2E). Collectively, the genetic mapping and rescue results demonstrate that the microglia defect in *biluo* mutants is caused by this T to I mutation in the *mcoln1a* gene.

The Aberrant Microglia Morphology in *biluo* Mutants Is Attributed to the Failure of Late Endosome and Lysosome Fusion

Previous studies in the fibroblasts from human patients with ML-IV and in the fat bodies of *mcoln1*-deficient drosophila have shown that MCOLN1 plays a critical role in the fusion of phagosomes and lysosomes in the

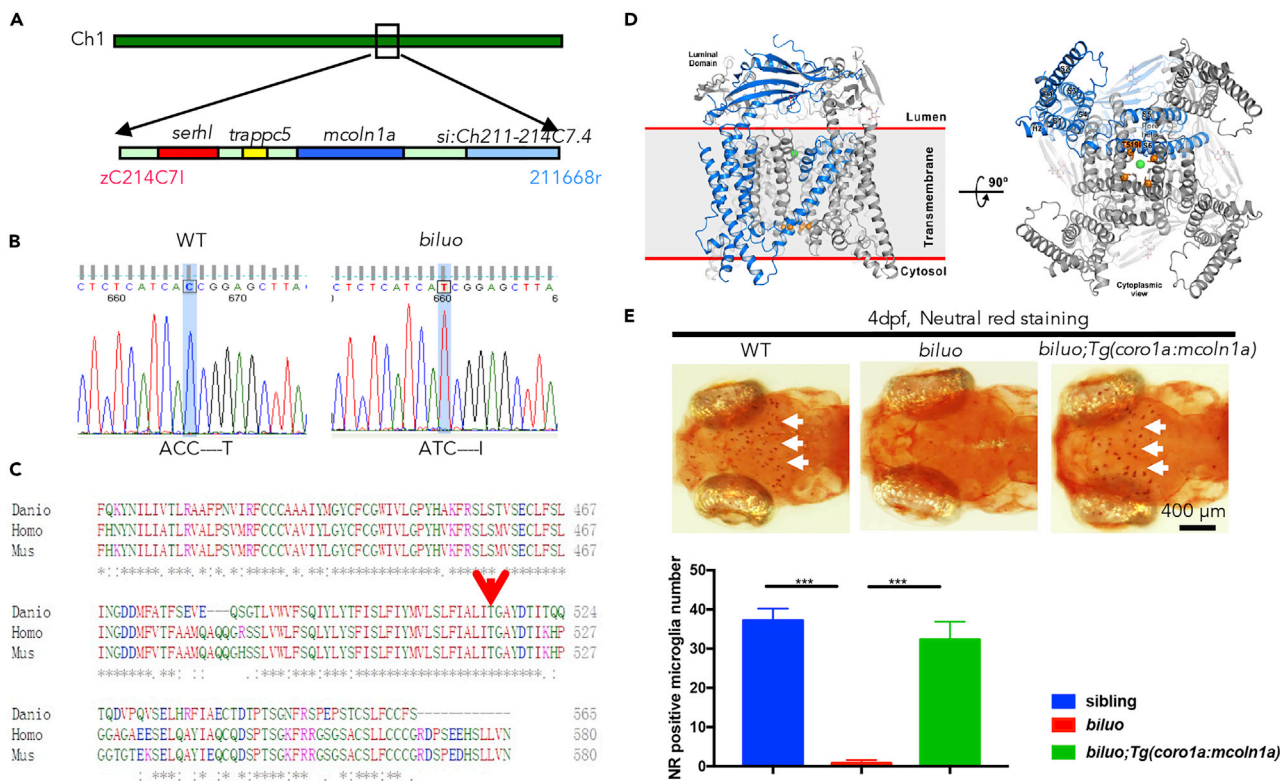


Figure 2. The Microglia Defect in *biluo* Mutants Is Caused by a Point Mutation in *mcoln1a*

(A) Positional cloning maps the *biluo* mutation to an 82-kb region on chromosome 1 between two SSLP markers, zC214C7I and 211668r. This region contains four genes: *serhl*, *trappc5*, *mcoln1a*, and *si:Ch211-214C7.4*.

(B) Sequencing the coding regions of the four candidate genes revealed a C to T point mutation in the *mcoln1a* gene, which leads to the change of amino acid T519 to (I).

(C) Alignment of human (*Homo*) MCOLN1, mouse (*Mus*) MCOLN1, and zebrafish (*Danio*) *Mcoln1a* protein sequence. Red arrow indicates the conserved 519th Threonine.

(D) 3D structural model of Mcoln1a channel. Green dot represents the central pore, and orange dots indicate the amino acid T519, which is mutated to I in *biluo* mutants.

(E) Neutral red (NR) staining of 4-dpf *Tg(coro1a:mcoln1a);biluo* embryos indicates that the neutral red staining defect of microglia in *biluo* mutants can be rescued by ectopically expressing WT *mcoln1a* in microglia. White arrows represent microglia. Quantification data of neutral-red-positive microglia number in 4-dpf siblings, *biluo* mutants, and *biluo;Tg(coro1a:mcoln1a)* embryos. $n(\text{ sibling}) = 5$ embryos, $n(\text{ biluo}) = 5$ embryos, $n(\text{ biluo;Tg(coro1a:mcoln1a)}) = 5$ embryos. *** $p < 0.001$. ANOVA. Error bars represent mean \pm SD.

endocytosis traffic pathway (Chen et al., 1998; Wong et al., 2012). We therefore hypothesized that the accumulation of enlarged phagosomes in *biluo* mutant microglia was possibly due to the impairment of the late endosome and lysosome fusion. To support this hypothesis, we conducted Lysotracker DND-99 staining on 4-dpf *Tg(coro1a:GFP);biluo* mutants and found that mutant microglia contained a significant increase of acid phagosomes in both number and diameter, which could be rescued by the reconstitution of WT *Mcoln1a* in microglia (Figures 3A and 3B). In contrast to *mcoln1ab* double-mutant zebrafish, MCOLN1-null mice, and *mcoln1*-deficient drosophila (Folkert et al., 1995; Li et al., 2017; Wakabayashi et al., 2011), neither phagosome accumulation nor excessive cell death was detected in the neurons of *biluo* mutants during early development (Figures S2 and S3), suggesting a redundant role of *mcoln1b*. To confirm the enlarged phagosome phenotype in mutant microglia was indeed caused by the impaired late endosome and lysosome fusion, we injected pH2A:GFP-Rab7 DNA construct, in which the expression of late-endosome marker GFP-Rab7 fusion protein was under the control of the H2A promoter (Clark et al., 2011), into *biluo* mutants and siblings at one-cell stage. The embryos survived to 3 dpf and were stained with anti-GFP, anti-Lcp1, and anti-LAMP1 antibodies to monitor the formation of late endosomes (GFP) and lysosomes (LAMP1) and their subsequent fusion in microglia (Lcp1 positive) (Herbomel et al., 1999; Jin et al., 2012). As shown in Figure 3, the late endosomes (green, indicated by arrows) in the microglia of siblings were relatively small with condensed bright GFP signals and they were co-localized with the lysosomes

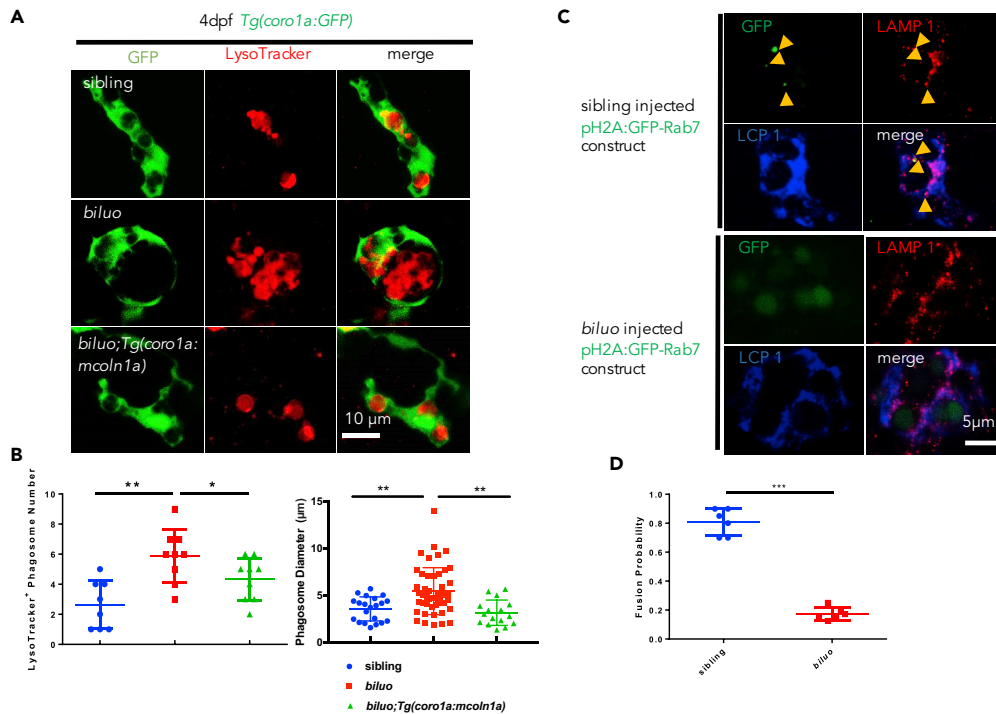


Figure 3. The Late Endosome and Lysosome Fusion Is Impaired in the *biluo* Microglia

(A) Fluorescent imaging (green) and LysoTracker staining of 4-dpf sibling, *biluo*, and *Tg(coro1a:mcoln1a);biluo* embryos show that the accumulation of acid phagosomes in *biluo* mutant microglia (middle panel) and morphological defect of microglia in *biluo* mutants can be rescued by ectopically expressing WT *mcoln1a* in microglia (lower panel).

(B) Quantification of the number and diameter of LysoTracker-positive phagosomes in the microglia in 4-dpf *Tg(coro1a:GFP)* siblings (blue dots), *Tg(coro1a:GFP);biluo* mutants (red squares), and *Tg(coro1a:mcoln1a);biluo* embryos (green triangles). n(sibling) = 8 microglia from 5 embryos; n(biluo) = 9 microglia from 5 embryos; n(*Tg(coro1a:mcoln1a);biluo*) = 9 microglia from 5 embryos. **p < 0.01, *p < 0.05, ANOVA. Error bars represent mean \pm SD.

(C) Anti-GFP (green), anti-LAMP1, and anti-Lcp1 (blue) triple antibody staining of WT embryos injected H2A:GFP-Rab7. Upper panels represent WT microglia (blue); late endosomes (green) are co-localized with the lysosomes. Lower panels represent mutant microglia (blue); late endosomes (green) are not co-localized with lysosomes.

(D) Quantification of fusion probability of late endosomes and lysosomes in sibling microglia (blue dots) and mutant microglia (red squares). n(sibling) = 6 microglia from 4 embryos, n(biluo) = 6 microglia from 4 embryos. ***p < 0.001. Error bars represent mean \pm SD.

(Figure 3C, upper panels), indicating successful fusion of the late endosomes and lysosomes. However, in the *biluo* mutant microglia, the late endosomes (green) were significantly enlarged with diffused faint GFP signals and they were clearly not co-localized with the lysosomes (Figure 3C, lower panels), indicating that late endosome and lysosome fusion is severely impaired in the mutant microglia. Quantification analysis showed that fusion between late endosomes and lysosomes was reduced for several-fold in *biluo* mutant microglia (Figure 3D). These data indicate that the aberrant morphology of microglia in *biluo* mutants is due to the failure of the late endosome and lysosome fusion, resulting in the accumulation of enlarged phagosomes in the cytosol. Because neutral red dyes are known to be enriched in the lysosomes through binding to lysosomal enzymes that are actively synthesized during phagocytosis (Chen et al., 1998), the failure of late endosome and lysosome fusion will likely interfere with the synthesis of the lysosomal enzymes, which leads to the reduction of neutral red staining in the *biluo* mutant microglia.

The Impairment of *Mcoln1a*-Mediated Ca²⁺ Release Causes the Blockage of Late Endosome and Lysosome Fusion in *biluo* Mutant Microglia

As shown in the 3D structure model, the side chain of T519 faces the central ion permeation pore of the lower gate (Figure 2D), which directly contributes to ion release of the channel (Chen et al., 2017;

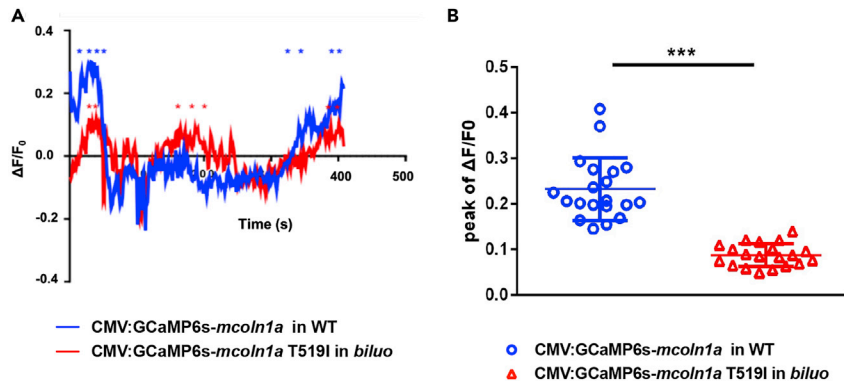


Figure 4. The T519 to I Mutation Reduces Mcoln1a-Mediated Ca^{2+} Efflux

(A) Representative calcium efflux of WT (blue) and mutant Mcoln1a channel. Stars represent calcium peaks we quantified. (B) Quantification of the mean of the peak of $\Delta F/F_0$ (representing Trpm1a-mediated Ca^{2+} efflux) in the macrophages in WT embryos injected with WT CMV:GCAMP6s-mcoln1a construct (blue dots) and the macrophages in biluo mutants injected with mutant CMV:GCAMP6s-mcoln1aT519I (red triangles). $\Delta F/F_0$ is calculated as $(F-F_0)/F_0$, where F_0 is the baseline fluorescence signal. Error bars represent mean \pm SD. n(WT late endosome) = 20 from 8 macrophages, n(biluo late endosome) = 20 from 7 macrophages.

Schmiege et al., 2017). We therefore speculated that, upon the replacement of Threonine by Isoleucine at residue 519, the hydrophobic side chain of Isoleucine might reduce the diameter of the central pore, thereby interfering with the calcium release of the channel. To test this hypothesis, we generated two constructions, CMV-GCaMP6s-mcoln1a and CMV-GCaMP6s-mcoln1aT519I, in which the calcium reporter GCaMP6s (Chen et al., 2013) was fused to the cytosolic N-terminal of WT Mcoln1a and mutant Mcoln1aT519I. The CMV-GCaMP6s-mcoln1a and CMV-GCaMP6s-mcoln1aT519I constructs were injected into one-cell stage WT and biluo embryos, respectively. The expression pattern and calcium efflux of WT Mcoln1a and Mcoln1aT519I mutant proteins were determined at around 2.5 dpf. Results showed that the GCaMP6s signals were co-localized with Lysotracker in the embryos injected with either WT Mcoln1a or mutant Mcoln1aT519I (Figure S4A), indicating that both WT GCaMP6s-Mcoln1a and mutant GCaMP6s-Mcoln1aT519I fusion proteins can properly target to the late endosomes and lysosomes. To monitor the function of WT and mutant Mcoln1a channels, we recorded the calcium efflux released from the late endosome in macrophages in the embryos injected with WT CMV-GCaMP6s-mcoln1a and mutant CMV-GCaMP6s-mcoln1aT519I constructs (Figure 4A). Quantification of the peak $\Delta F/F_0$ value ($\Delta F/F_0$) was calculated as $(F-F_0)/F_0$, where F_0 is the baseline fluorescence signal per late endosome showed that the calcium efflux mediated by Mcoln1aT519I mutant proteins was 2.5-fold lower than that of WT Mcoln1a (Figure 4B). To exclude the background effect of abnormal lysosomes/endosomes in the mutant microglia, we overexpressed WT GCAMP-Mcoln1a and mutant GCAMP-Mcoln1aT519 in WT embryos and monitored the calcium efflux in WT macrophages. Results showed that the calcium efflux mediated by Mcoln1aT519I was also significantly reduced (Figure S4B). These data indicate that the blockade of the late endosome and lysosome fusion in biluo mutant microglia is likely attributed to the reduction of calcium released from the Mcoln1a channel.

Aberrant Microglial Function Leads to Excessive Neuronal Activities in Biluo Mutants

It is well known that mutations in the MCOLN1 gene in humans cause ML-IV disorder, a neurodegenerative and lysosomal storage disorder with various neuronal symptoms, including psychomotor retardation and vision impairment (Bargal et al., 2000; Bassi et al., 2000; Wakabayashi et al., 2011). Animal model studies in mice, fish, and fly have shown that these various neuronal symptoms are believed to be caused, at least in part, by the intrinsic defects in the neurons (Li et al., 2017; Micsenyi et al., 2009; Venkatachalam et al., 2008; Venugopal et al., 2007). Yet, the role of microglia in ML-IV disorder remains elusive, despite the fact that microglia exhibit abnormal morphology in human patients with ML-IV and MCOLN1-deficient mice (Folkert et al., 1995). Given the fact that biluo mutant microglia display an aberrant morphology similar to those in human patients with ML-IV, the mutant fish provide a useful platform to address this question. Because biluo is a hypomorphic mutant and neuronal behavior study is less established in adult zebrafish, we decided to examine the spontaneous and

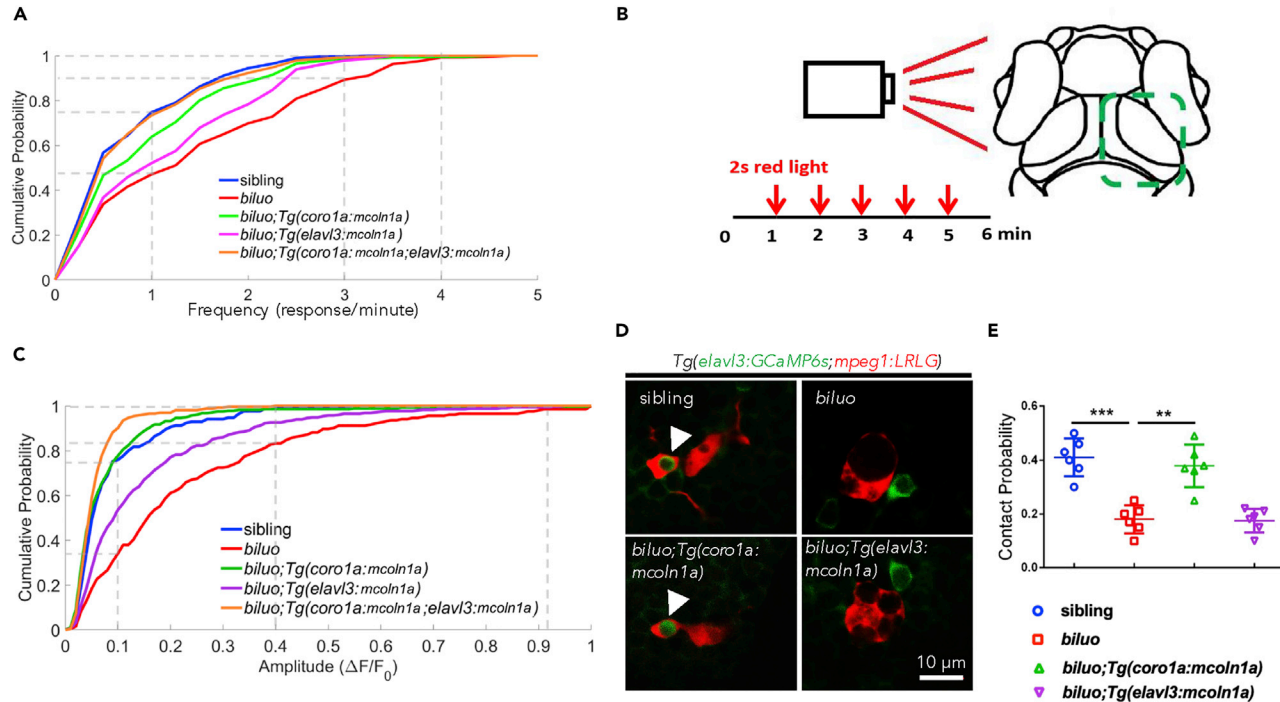


Figure 5. Optic Tectal Neurons in *biluo* Mutants Exhibit Excessive Spontaneous and Visual-Evoked Activities

(A) Distribution of frequency of spontaneous responses of the tectal neurons in sibling, *biluo*, *biluo;Tg(coro1a:mcoln1a)*, *biluo;Tg(elavl3:mcoln1a)*, and *biluo;Tg(coro1a:mcoln1a;elavl3:mcoln1a)*. n(sibling) = 214 cells in 4 embryos, n(biluo) = 166 cells in 4 embryos, n(biluo; *Tg(coro1a:mcoln1a)*) = 165 cells in 4 embryos, n(biluo; *Tg(elavl3:mcoln1a)*) = 221 cells in 5 embryos and n(*biluo;Tg(coro1a:mcoln1a;elavl3:mcoln1a)*) = 225 cells in 4 embryos. P(sibling vs biluo) = 4.6×10^{-13} , P(biluo vs *biluo;Tg(coro1a:mcoln1a)*) = 9.4×10^{-6} , P(biluo vs *biluo;Tg(elavl3:mcoln1a)*) = 0.0017, and P(biluo vs *biluo;Tg(coro1a:mcoln1a;elavl3:mcoln1a)*) = 5.7×10^{-10} .

(B) Schematic of recording visual-evoked responses of optic tectal neurons in 6-dpf embryos. Red light flashed was given to the left eye of the embryos at 1, 2, 3, 4, and 5 min, and the duration of each stimulus was 2 s. The neuronal responses of the right half tectum were recorded.

(C) Distribution of average peak of $\Delta F/F_0$ in sibling, *biluo*, *biluo;Tg(coro1a:mcoln1a)*, *biluo;Tg(elavl3:mcoln1a)*, and *biluo;Tg(coro1a:mcoln1a;elavl3:mcoln1a)*. n(sibling) = 203 cells in 4 embryos, n(biluo) = 263 cells in 4 embryos, n(biluo; *Tg(coro1a:mcoln1a)*) = 305 cells in 4 embryos, n(biluo; *Tg(elavl3:mcoln1a)*) = 364 cells in 5 embryos, n(*biluo;Tg(coro1a:mcoln1a;elavl3:mcoln1a)*) = 280 cells in 4 embryos. P(sibling vs biluo) = 4.9×10^{-17} , P(biluo vs *biluo;Tg(coro1a:mcoln1a)*) = 4.7×10^{-22} , P(biluo vs *biluo;Tg(elavl3:mcoln1a)*) = 4.2×10^{-6} , P(biluo vs *biluo;Tg(coro1a:mcoln1a;elavl3:mcoln1a)*) = 3.2×10^{-34} , and P(biluo; *Tg(coro1a:mcoln1a)* vs *biluo;Tg(elavl3:mcoln1a)*) = 2.1×10^{-11} .

(D) Representative images of neuron (green)-microglia contact in 5-dpf sibling, *biluo*, *biluo;Tg(coro1a:mcoln1a)*, and *biluo;Tg(elavl3:mcoln1a)* embryos.

(E) Quantification of contact probability between microglia and optic tectal neurons. Contact duration longer than 24 s is recognized as a functional microglia-neuron contact. n(sibling) = 9 embryos, n(biluo) = 10 embryos, n(*biluo;Tg(coro1a:mcoln1a)*) = 9 embryos, n(*biluo;Tg(elavl3:mcoln1a)*) = 8 embryos. ***p < 0.0001, **p < 0.001, ANOVA. Error bars represent mean \pm SD.

visual-evoked neuronal activities, both of which have been shown to be modulated by microglia at early developmental stage (Li et al., 2012b), in *biluo* mutants. We crossed *Tg(elavl3:GCaMP6s)* line, in which the calcium indicator GCaMP6s is selectively expressed in the neurons, with *biluo* mutants as well as three different mutant transgenic lines, *biluo;Tg(coro1a:mcoln1a)*, *biluo;Tg(elavl3:mcoln1a)*, and *biluo;Tg(coro1a:mcoln1a;elavl3:mcoln1a)*, ectopically expressing WT *mcoln1a* in microglia and neurons alone or together (Figures S1 and S5). At 6 dpf, the neuronal activities in the optic tectum, where microglia predominantly reside in developing zebrafish brain (Xu et al., 2015, 2016), were analyzed under both non-stimulated and visual-evoked conditions. For spontaneous neuronal activity, we calculated the frequency of calcium events per neuron and plotted the cumulative curves for the distribution of neuronal frequency (Figure 5A). In control siblings, more than 70% of the neurons showed one event or less per minute and none of the neurons exhibited three to four events per minute (Figure 5A). Intriguingly, in *biluo* mutants, 10% of the tectal neurons had three to four events per minute and the neurons with the frequency less than one event per minute were reduced to 50% (Figure 5A), indicating that the optic tectal neurons in *biluo* mutants display excessive spontaneous activities. Remarkably, these excessive neuronal activities were partially rescued by ectopically expressing WT *mcoln1a* in

either neurons or microglia and were fully rescued by expressing WT *mcoln1a* in the neurons and microglia together (Figure 5A).

We next explored the visual-evoked activities of the tectal neurons in *biluo* mutants by recording the neuronal activities on the contralateral optic tectum after stimulating the larva with one-side red light flashes lasting for 2 s for five times with 1-min intervals (Figure 5B). To quantify the visual-evoked responses of tectal neurons, we averaged the five-time responses (5 s after stimulus) for each neuron by averaging the peak of $\Delta F/F_0$ ($\Delta F/F_0$ was calculated as $(F-F_0)/F_0$, where F_0 is average fluorescence during 5 s before stimulus). The cumulative curves for the distribution of the peaks of tectal neuron's responses in siblings, *biluo*, *biluo;Tg(coro1a:mcoln1a)*, *biluo;Tg(elavl3:mcoln1a)* and *biluo;Tg(coro1a:mcoln1a;elavl3:mcoln1a)* mutants, were plotted (Figure 5C). Results showed that, similar to the spontaneous neuronal activity, the visual-evoked tectal responses were also significantly higher in *biluo* mutants and these excessive neuronal responses could be rescued by ectopically expressing WT *mcoln1a* in microglia. Taken together, these data indicate that, in addition to the intrinsic neuronal impairment, aberrant microglial function also contributes to the dysregulation of neuronal activities in *mcoln1a*-deficient fish.

Previous study by Li et al. have reported that microglia preferentially interact with highly activated neurons by wrapping around their soma into a bulbous structure, leading to the reduction of the activities of these neurons (Li et al., 2012b). We therefore hypothesized that the excessive neuronal activities in *biluo* mutants might be due to the impairment of the neuron-microglia interaction. Based on previous study (Li et al., 2012b), a functional neuron-microglia contact will be achieved when microglia form a bulbous structure on a neuron soma for more than 24 s. We therefore compared the contact probability between the tectal neurons and microglia in the optic tectum of siblings, *biluo*, *biluo;Tg(coro1a:mcoln1a)*, and *biluo;Tg(elavl3:mcoln1a)* mutant fish. Results showed that the probability of functional neuron-microglia contacts in *biluo* mutants was about a half of that in siblings (Figures 5D and 5E). This impaired contact probability in *biluo* mutants was restored by ectopically expressing WT *Mcoln1a* in microglia but not in neurons (Figures 5D and 5E). Collectively, these results indicate that the excessive neuronal activities of the tectal neurons in *biluo* mutants is attributed, at least in part, to the impairment of direct interaction between neurons and microglia.

DISCUSSION

In this study, we reported the identification and characterization of a zebrafish mutant *biluo*, which harbors a hypomorphic mutation in the *mcoln1a* gene, one of the two zebrafish homologs of mammalian *MCOLN1*. Our study showed that loss of *Mcoln1a* function impairs the microglia-neuron interaction, resulting in excessive neuronal activities.

It is well known that mutations in the *MCOLN1* gene in human cause type IV mucolipidosis (ML-IV), a neurodegenerative and lysosomal storage disorder that displays various neurological symptoms (Bargal et al., 2001; Bassi et al., 2000; Wakabayashi et al., 2011). The hallmark of ML-IV disease is that the patients often suffer from progressive psychomotor retardation, especially their movement and coordination, in an age-dependent manner (Bach, 2001). However, we did not observe excessive neuronal cell death, movement, and coordination defects in *biluo* mutants (data not shown). This is likely attributed to the hypomorphic T to I mutation of *Mcoln1a* as well as the functional compensation of *Mcoln1b*, which shares 60% similarity in protein sequence with *Mcoln1a*. Indeed, excessive neuronal cell death was detected in the complete loss of *mcoln1a* function mutant fish and *mcoln1ab* double-deficient fish (Li et al., 2017). Further in-depth study will be required to clarify whether complete loss of *Mcoln1* function in zebrafish would lead to movement and coordination defects. Nevertheless, as missense mutations in the *MCOLN1* gene have been found to cause mild symptoms in human patients (Bargal et al., 2001; Reis et al., 1993), we believe that the *biluo* mutants may represent a mild ML-IV disease model for the mechanistic study of the disease and drug screening.

Although *biluo* mutants lack movement and coordination phenotypes, they exhibit excessive neuronal activities under spontaneous and visual-evoked conditions. These aberrant neuronal activities appear to be caused by the intrinsic defect of neurons as well as the extrinsic contribution from the microglia. Previous studies in the *mcoln1*-deficient drosophila have shown that the movement and coordination defects in the mutant fly are caused by excessive neuronal cell death (Venkatachalam et al., 2008). Intriguingly, no obvious abnormal neural cell death is observed in *biluo* mutants, suggesting that the abnormal neuronal activities in

biluo mutants is likely not caused by excessive neuronal cell death. It is known that the impairment of endosomal fusion pathway could interfere with the neurotransmitter recycling process (Rizzoli, 2014). The partial loss of *Mcoln1a* function could reduce the degradation of neurotransmitters in neurons due to the impaired fusion of transmitter vesicles with lysosomes. As a consequence, more neurotransmitters will be released to the post-synaptic membrane, resulting in a stronger spontaneous and visual-evoked neuronal response. Likewise, as microglia have also been implicated in the removal of neurotransmitters via phagocytosis (Shaked et al., 2005), the excessive spontaneous and visual-evoked neuronal activities in *biluo* mutants could contribute to the impairment of removing neurotransmitters by microglia. Indeed, when we injected bacteria into the brain of 4-dpf *biluo* mutant embryos, we found that the ability of engulfing the bacteria by the mutant microglia was significantly reduced (Figure S6). This observation supports the hypothesis that the excessive neuronal response in *biluo* mutants could be attributed to the impairment of neurotransmitter recycling.

Finally, previous studies have reported that aberrant microglia activity contribute to the onset and the progression of a number of neurodegenerative diseases, including Alzheimer and Parkinson diseases, Amyotrophic lateral sclerosis, and prion disease, presumably by releasing pro-inflammatory and neurotoxic factors (Block et al., 2007; Kim et al., 2015; Qin et al., 2004; Takeuchi et al., 2006; Thompson and Tsirka, 2017). Interestingly, our study shows that the aberrant microglial function caused by *mcoln1a* deficiency could lead to abnormal excessive neuronal activities. This finding suggests that microglia-neuron interaction may play a role in the development and progression of ML-IV disease as well as some other neurological disorders. One example is Fragile X syndrome (FXS), a type of Autism spectrum disorder caused by developmental defects in brain connectivity (Geschwind and Levitt, 2007). The FXS mouse model shows abnormal high synchrony in the firing of cortical neurons (Goncalves et al., 2013). It will be of great interest to explore the role of microglia in the FXS mouse model.

Limitations of the Study

This study has demonstrated that loss of *Mcoln1a* function in zebrafish impairs microglia-neuron interaction, which leads to excessive neuronal activities in the mutant animals. However, whether dysregulation of microglial function contributes to the development of type IV mucolipidosis needs to be further investigated in human patients.

METHODS

All methods can be found in the accompanying [Transparent Methods supplemental file](#).

SUPPLEMENTAL INFORMATION

Supplemental Information can be found online at <https://doi.org/10.1016/j.isci.2019.02.031>.

ACKNOWLEDGMENTS

We thank Dr. Brian A. Link (Medical College of Wisconsin, USA) for providing the H2A: GFP-Rab7 construct. We also like to thank Dr. Sicong He and Dr. Jianan Y. Qu for their help in the infrared laser system. This work was supported by the National Natural Science Foundation of China (31761163008), the General Research Fund from the Research Grants Council of the HKSAR (16103515; 16102617; N_HKUST621/17; AoE/M-09/12), and the Innovation and Technology Commission of the HKSAR (ITCPD/17-9).

AUTHOR CONTRIBUTIONS

W.J., Y.D., F.L., L.Z., Z.H., W.L. and J.L. performed experiments. W.J., Y.D., L.Z., M.Z., J.D., M.Z., W.Z. and Z.W. designed experiments. W.J., Y.D., W.Z. and Z.W. wrote the manuscript.

DECLARATION OF INTERESTS

The authors declare no competing interests.

Received: July 9, 2018

Revised: October 28, 2018

Accepted: February 26, 2019

Published: March 29, 2019

REFERENCES

- Bach, G. (2001). Mucolipidosis type IV. *Mol. Genet. Metab.* 73, 197–203.
- Bach, G. (2005). Mucolipin 1: endocytosis and cation channel—a review. *Pflugers Arch.* 451, 313–317.
- Bargal, R., Avidan, N., Ben-Asher, E., Olander, Z., Zeigler, M., Frumkin, A., Raas-Rothschild, A., Glusman, G., Lancet, D., and Bach, G. (2000). Identification of the gene causing mucolipidosis type IV. *Nat. Genet.* 26, 118–123.
- Bargal, R., Avidan, N., Olander, T., Ben Asher, E., Zeigler, M., Raas-Rothschild, A., Frumkin, A., Ben-Yoseph, O., Friedlander, Y., Lancet, D., et al. (2001). Mucolipidosis type IV: novel MCOLN1 mutations in Jewish and non-Jewish patients and the frequency of the disease in the Ashkenazi Jewish population. *Hum. Mutat.* 17, 397–402.
- Bassi, M.T., Manzoni, M., Monti, E., Pizzo, M.T., Ballabio, A., and Borsani, G. (2000). Cloning of the gene encoding a novel integral membrane protein, mucolipin-1 and identification of the two major founder mutations causing mucolipidosis type IV. *Am. J. Hum. Genet.* 67, 1110–1120.
- Bialas, A.R., and Stevens, B. (2013). TGF-beta signaling regulates neuronal C1q expression and developmental synaptic refinement. *Nat. Neurosci.* 16, 1773–1782.
- Block, M.L., Zecca, L., and Hong, J.S. (2007). Microglia-mediated neurotoxicity: uncovering the molecular mechanisms. *Nat. Rev. Neurosci.* 8, 57–69.
- Casano, A.M., and Peri, F. (2015). Microglia: multitasking specialists of the brain. *Dev. Cell* 32, 469–477.
- Casano, A.M., Albert, M., and Peri, F. (2016). Developmental apoptosis mediates entry and positioning of microglia in the zebrafish brain. *Cell Rep.* 16, 897–906.
- Chastain, E.M., Duncan, D.S., Rodgers, J.M., and Miller, S.D. (2011). The role of antigen presenting cells in multiple sclerosis. *Biochim. Biophys. Acta* 1812, 265–274.
- Chen, C.S., Bach, G., and Pagano, R.E. (1998). Abnormal transport along the lysosomal pathway in mucolipidosis, type IV disease. *Proc. Natl. Acad. Sci. U S A* 95, 6373–6378.
- Chen, Q., She, J., Zeng, W., Guo, J., Xu, H., Bai, X.C., and Jiang, Y. (2017). Structure of mammalian endolysosomal TRPML1 channel in nanodiscs. *Nature* 550, 415–418.
- Chen, T.W., Wardill, T.J., Sun, Y., Pulver, S.R., Renninger, S.L., Baohan, A., Schreiter, E.R., Kerr, R.A., Orger, M.B., Jayaraman, V., et al. (2013). Ultrasensitive fluorescent proteins for imaging neuronal activity. *Nature* 499, 295–300.
- Clark, B.S., Winter, M., Cohen, A.R., and Link, B.A. (2011). Generation of Rab-based transgenic lines for *in vivo* studies of endosome biology in zebrafish. *Dev. Dyn.* 240, 2452–2465.
- Davoust, N., Vuaillet, C., Androdias, G., and Nataf, S. (2008). From bone marrow to microglia: barriers and avenues. *Trends Immunol.* 29, 227–234.
- Derecki, N.C., Cronk, J.C., Lu, Z., Xu, E., Abbott, S.B., Guyenet, P.G., and Kipnis, J. (2012). Wild-type microglia arrest pathology in a mouse model of Rett syndrome. *Nature* 484, 105–109.
- Dong, X.P., Cheng, X., Mills, E., Delling, M., Wang, F., Kurz, T., and Xu, H. (2008). The type IV mucolipidosis-associated protein TRPML1 is an endolysosomal iron release channel. *Nature* 455, 992–996.
- Dong, X.P., Wang, X., Shen, D., Chen, S., Liu, M., Wang, Y., Mills, E., Cheng, X., Delling, M., and Xu, H. (2009). Activating mutations of the TRPML1 channel revealed by proline-scanning mutagenesis. *J. Biol. Chem.* 284, 32040–32052.
- Dong, X.P., Wang, X., and Xu, H. (2010). TRP channels of intracellular membranes. *J. Neurochem.* 113, 313–328.
- Driever, W., Solnica-Krezel, L., Schier, A.F., Neuhauss, S.C., Malicki, J., Stemple, D.L., Stainier, D.Y., Zwartkruis, F., Abdelilah, S., Rangini, Z., et al. (1996). A genetic screen for mutations affecting embryogenesis in zebrafish. *Development* 123, 37–46.
- Folkert, R.D., Alroy, J., Lomakina, I., Skutelsky, E., Raghavan, S.S., and Kolodny, E.H. (1995). Mucolipidosis IV: morphology and histochemistry of an autopsy case. *J. Neuropathol. Exp. Neurol.* 54, 154–164.
- Geschwind, D.H., and Levitt, P. (2007). Autism spectrum disorders: developmental disconnection syndromes. *Curr. Opin. Neurobiol.* 17, 103–111.
- Goncalves, J.T., Anstey, J.E., Golshani, P., and Portera-Cailliau, C. (2013). Circuit level defects in the developing neocortex of Fragile X mice. *Nat. Neurosci.* 16, 903–909.
- Graeber, M.B., and Streit, W.J. (2010). Microglia: biology and pathology. *Acta Neuropathol.* 119, 89–105.
- Haffter, P., Granato, M., Brand, M., Mullins, M.C., Hammerschmidt, M., Kane, D.A., Odenthal, J., van Eeden, F.J., Jiang, Y.J., Heisenberg, C.P., et al. (1996). The identification of genes with unique and essential functions in the development of the zebrafish, *Danio rerio*. *Development* 123, 1–36.
- Hanisch, U.K., and Kettenmann, H. (2007). Microglia: active sensor and versatile effector cells in the normal and pathologic brain. *Nat. Neurosci.* 10, 1387–1394.
- Herbomel, P., Thisse, B., and Thisse, C. (1999). Ontogeny and behaviour of early macrophages in the zebrafish embryo. *Development* 126, 3735–3745.
- Herbomel, P., Thisse, B., and Thisse, C. (2001). Zebrafish early macrophages colonize cephalic mesenchyme and developing brain, retina, and epidermis through a M-CSF receptor-dependent invasive process. *Dev. Biol.* 238, 274–288.
- Herz, J., Filiano, A.J., Smith, A., Yogev, N., and Kipnis, J. (2017). Myeloid cells in the central nervous system. *Immunity* 46, 943–956.
- Hickman, S.E., Allison, E.K., and El Khoury, J. (2008). Microglial dysfunction and defective beta-amyloid clearance pathways in aging Alzheimer's disease mice. *J. Neurosci.* 28, 8354–8360.
- Hortega, d.R. (1919). El tercer elemento de los centros nerviosos. *Bol. Soc. Esp. Biol.* 9, 69–129.
- Iaccarino, H.F., Singer, A.C., Martorell, A.J., Rudenko, A., Gao, F., Gillingham, T.Z., Mathys, H., Seo, J., Kritskiy, O., Abdurrob, F., et al. (2016). Gamma frequency entrainment attenuates amyloid load and modifies microglia. *Nature* 540, 230–235.
- Jin, H., Li, L., Xu, J., Zhen, F., Zhu, L., Liu, P.P., Zhang, M., Zhang, W., and Wen, Z. (2012). Runx1 regulates embryonic myeloid fate choice in zebrafish through a negative feedback loop inhibiting Pu.1 expression. *Blood* 119, 5239–5249.
- Kim, G.H., Kim, J.E., Rhee, S.J., and Yoon, S. (2015). The role of oxidative stress in neurodegenerative diseases. *Exp. Neurobiol.* 24, 325–340.
- Kim, S.U., and de Vellis, J. (2005). Microglia in health and disease. *J. Neurosci. Res.* 81, 302–313.
- Kreutzberg, G.W. (1995). Microglia, the first line of defence in brain pathologies. *Arzneimittelforschung* 45, 357–360.
- LaPlante, J.M., Falardeau, J., Sun, M., Kanazirska, M., Brown, E.M., Slaugenhoupt, S.A., and Vassilev, P.M. (2002). Identification and characterization of the single channel function of human mucolipin-1 implicated in mucolipidosis type IV, a disorder affecting the lysosomal pathway. *FEBS Lett.* 532, 183–187.
- LaPlante, J.M., Ye, C.P., Quinn, S.J., Goldin, E., Brown, E.M., Slaugenhoupt, S.A., and Vassilev, P.M. (2004). Functional links between mucolipin-1 and Ca²⁺-dependent membrane trafficking in mucolipidosis IV. *Biochem. Biophys. Res. Commun.* 322, 1384–1391.
- Li, H., Pei, W., Vergara-Jauregui, S., Zerfas, P.M., Raben, N., Burgess, S.M., and Puertollano, R. (2017). Novel degenerative and developmental defects in a zebrafish model of mucolipidosis type IV. *Hum. Mol. Genet.* 26, 2701–2718.
- Li, L., Yan, B., Shi, Y.Q., Zhang, W.Q., and Wen, Z.L. (2012a). Live imaging reveals differing roles of macrophages and neutrophils during zebrafish tail fin regeneration. *J. Biol. Chem.* 287, 25353–25360.
- Li, Y., Du, X.F., Liu, C.S., Wen, Z.L., and Du, J.L. (2012b). Reciprocal regulation between resting microglial dynamics and neuronal activity *in vivo*. *Dev. Cell* 23, 1189–1202.
- Luzio, J.P., Bright, N.A., and Pryor, P.R. (2007). The role of calcium and other ions in sorting and delivery in the late endocytic pathway. *Biochem. Soc. Trans.* 35, 1088–1091.
- Manzoni, M., Monti, E., Bresciani, R., Bozzato, A., Barlati, S., Bassi, M.T., and Borsani, G. (2004). Overexpression of wild-type and mutant mucolipin proteins in mammalian cells: effects on the late endocytic compartment organization. *FEBS Lett.* 567, 219–224.

- Micsenyi, M.C., Dobrenis, K., Stephney, G., Pickel, J., Vanier, M.T., Slaugenhoupt, S.A., and Walkley, S.U. (2009). Neuropathology of the *Mcoln1(-/-)* knockout mouse model of mucolipidosis type IV. *J. Neuropathol. Exp. Neurol.* 68, 125–135.
- Morgan, A.J., Platt, F.M., Lloyd-Evans, E., and Galione, A. (2011). Molecular mechanisms of endolysosomal Ca²⁺ signalling in health and disease. *Biochem. J.* 439, 349–374.
- Napoli, I., and Neumann, H. (2009). Microglial clearance function in health and disease. *Neuroscience* 158, 1030–1038.
- Paolicelli, R.C., Bolasco, G., Pagani, F., Maggi, L., Scianni, M., Panzanelli, P., Giustetto, M., Ferreira, T.A., Guiducci, E., Dumas, L., et al. (2011). Synaptic pruning by microglia is necessary for normal brain development. *Science* 333, 1456–1458.
- Peri, F., and Nusslein-Volhard, C. (2008). Live imaging of neuronal degradation by microglia reveals a role for v0-ATPase a1 in phagosomal fusion in vivo. *Cell* 133, 916–927.
- Ponomarev, E.D., Shriver, L.P., Maresz, K., and Dittel, B.N. (2005). Microglial cell activation and proliferation precedes the onset of CNS autoimmunity. *J. Neurosci. Res.* 81, 374–389.
- Qin, L., Liu, Y., Wang, T., Wei, S.J., Block, M.L., Wilson, B., Liu, B., and Hong, J.S. (2004). NADPH oxidase mediates lipopolysaccharide-induced neurotoxicity and proinflammatory gene expression in activated microglia. *J. Biol. Chem.* 279, 1415–1421.
- Reis, S., Sheffer, R.N., Merin, S., Luder, A.S., and Bach, G. (1993). Mucolipidosis type IV: a mild form with late onset. *Am. J. Med. Genet.* 47, 392–394.
- Rizzoli, S.O. (2014). Synaptic vesicle recycling: steps and principles. *EMBO J.* 33, 788–822.
- Schafer, D.P., Lehrman, E.K., Kautzman, A.G., Koyama, R., Mardinaly, A.R., Yamasaki, R., Ransohoff, R.M., Greenberg, M.E., Barres, B.A., and Stevens, B. (2012). Microglia sculpt postnatal neural circuits in an activity and complement-dependent manner. *Neuron* 74, 691–705.
- Schmiege, P., Fine, M., Blobel, G., and Li, X. (2017). Human TRPML1 channel structures in open and closed conformations. *Nature* 550, 366–370.
- Shaked, I., Tchoresh, D., Gersner, R., Meiri, G., Mordechai, S., Xiao, X., Hart, R.P., and Schwartz, M. (2005). Protective autoimmunity: interferon-gamma enables microglia to remove glutamate without evoking inflammatory mediators. *J. Neurochem.* 92, 997–1009.
- Squarezoni, P., Oller, G., Hoeffel, G., Pont-Lezica, L., Rostaing, P., Low, D., Bessis, A., Ginhoux, F., and Garel, S. (2014). Microglia modulate wiring of the embryonic forebrain. *Cell Rep.* 8, 1271–1279.
- Takeuchi, H., Jin, S., Wang, J., Zhang, G., Kawanokuchi, J., Kuno, R., Sonobe, Y., Mizuno, T., and Suzumura, A. (2006). Tumor necrosis factor-alpha induces neurotoxicity via glutamate release from hemichannels of activated microglia in an autocrine manner. *J. Biol. Chem.* 281, 21362–21368.
- Thompson, K.K., and Tsirka, S.E. (2017). The diverse roles of microglia in the neurodegenerative aspects of central nervous system (CNS) autoimmunity. *Int. J. Mol. Sci.* 18, E504.
- Tremblay, M.E., Lowery, R.L., and Majewska, A.K. (2010). Microglial interactions with synapses are modulated by visual experience. *PLoS Biol.* 8, e1000527.
- Venkatachalam, K., Long, A.A., Elsaesser, R., Nikolaeva, D., Broadie, K., and Montell, C. (2008). Motor deficit in a *Drosophila* model of mucolipidosis type IV due to defective clearance of apoptotic cells. *Cell* 135, 838–851.
- Venugopal, B., Browning, M.F., Curcio-Morelli, C., Varro, A., Michaud, N., Nanthakumar, N., Walkley, S.U., Pickel, J., and Slaugenhoupt, S.A. (2007). Neurologic, gastric, and ophthalmologic pathologies in a murine model of mucolipidosis type IV. *Am. J. Hum. Genet.* 81, 1070–1083.
- Wakabayashi, K., Gustafson, A.M., Sidransky, E., and Goldin, E. (2011). Mucolipidosis type IV: an update. *Mol. Genet. Metab.* 104, 206–213.
- Wake, H., Moorhouse, A.J., Jinno, S., Kohsaka, S., and Nabekura, J. (2009). Resting microglia directly monitor the functional state of synapses *in vivo* and determine the fate of ischemic terminals. *J. Neurosci.* 29, 3974–3980.
- Walker, M.T., and Montell, C. (2016). Suppression of the motor deficit in a mucolipidosis type IV mouse model by bone marrow transplantation. *Hum. Mol. Genet.* 25, 2752–2761.
- Wong, C.O., Li, R., Montell, C., and Venkatachalam, K. (2012). *Drosophila* TRPML is required for TORC1 activation. *Curr. Biol.* 22, 1616–1621.
- Wu, S., Xue, R., Hassan, S., Nguyen, T.M.L., Wang, T., Pan, H., Xu, J., Liu, Q., Zhang, W., and Wen, Z. (2018). II34-Csf1r pathway regulates the migration and colonization of microglial precursors. *Dev. Cell* 46, 552–563.
- Xu, J., Zhu, L., He, S., Wu, Y., Jin, W., Yu, T., Qu, J.Y., and Wen, Z. (2015). Temporal-spatial resolution rate mapping reveals distinct origins for embryonic and adult microglia in zebrafish. *Dev. Cell* 34, 632–641.
- Xu, J., Wang, T., Wu, Y., Jin, W., and Wen, Z. (2016). Microglia colonization of developing zebrafish midbrain is promoted by apoptotic neuron and lysophosphatidylcholine. *Dev. Cell* 38, 214–222.

Supplemental Information

**Dysregulation of Microglial Function
Contributes to Neuronal Impairment
in *Mcoln1a*-Deficient Zebrafish**

Wan Jin, Yimei Dai, Funing Li, Lu Zhu, Zhibin Huang, Wei Liu, Jianchao Li, Mingjie Zhang, Jiulin Du, Wenqing Zhang, and Zilong Wen

SUPPLEMENTAL FIGURES AND LEGENDS

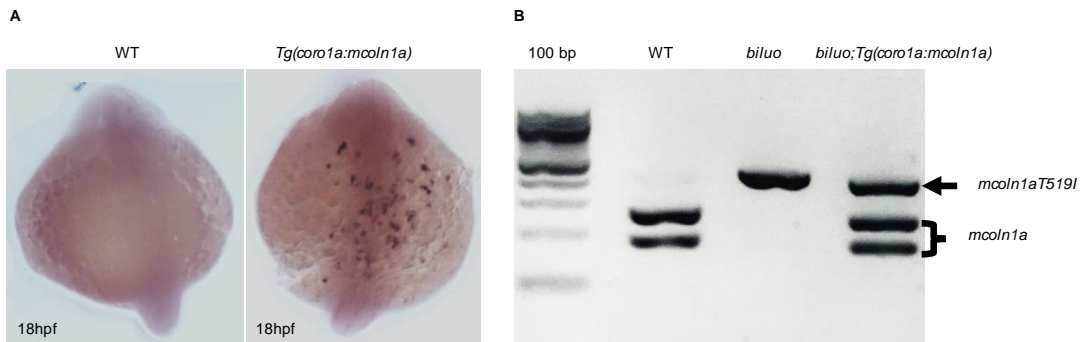


Figure S1 related to Figure 2. **The Expression of WT *mcoln1a* in *Tg(coro1a:mcoln1a)* Transgenic and *biluo;Tg(coro1a:mcoln1a)* Mutant Transgenic Embryos.**

(A) *In-situ* hybridization of *mcoln1a* in myeloid precursors in *Tg(coro1a:mcoln1a)* transgenic and control WT embryos at 18 hpf.

(B) The *mcoln1a* transcripts in microglia are detected by RT-PCR analysis of the microglia isolated from the brains of 3 dpf *Tg(mpeg1:LRLG)*, *biluo;Tg(mpeg1:LRLG)* and *biluo;Tg(coro1a:mcoln1a;mpeg1:LRLG)* embryos. The PCR product of WT *mcoln1a* can be cleaved into two smaller fragments (~200 bp) by MspI, whereas the PCR product of mutant *mcoln1a* is resistant to MspI digestion.

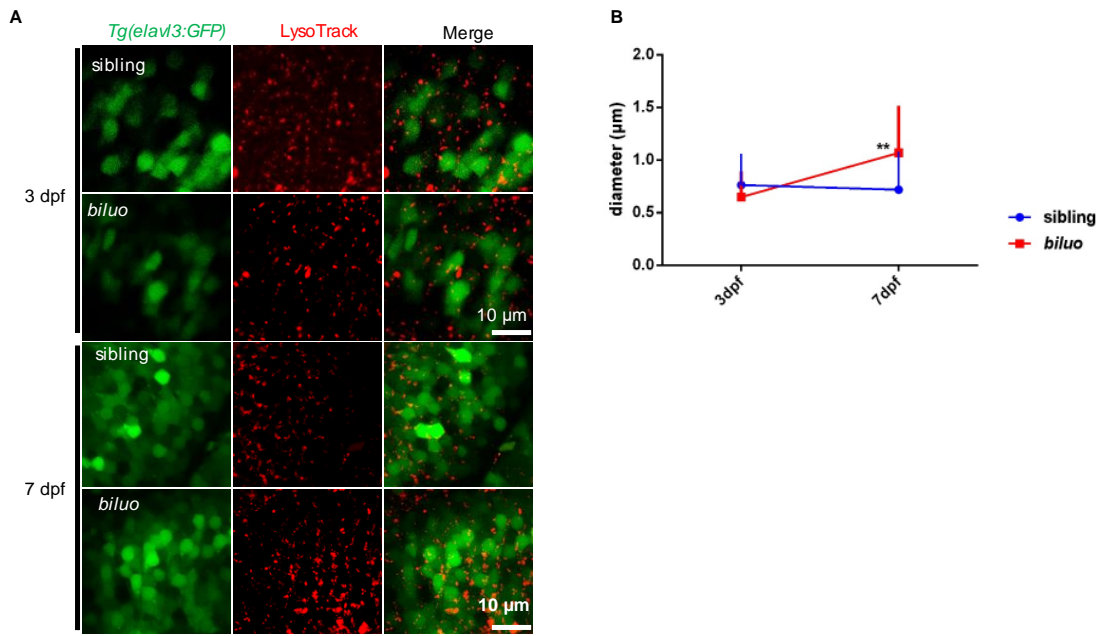


Figure S2 related to Figure 3. **Lysosomal Accumulation in the Neurons of *biluo* Mutants.**

- (A) Lysotracker staining (red) of neurons (green) in both *Tg(elavl3:GFP)* and *biluo;Tg(elavl3:GFP)* at 3 dpf (upper panels) and 7 dpf (lower panels).
- (B) Quantification data of the diameter of Lysotracker positive lysosomal accumulation. n(4 dpf sibling)=5 embryos, n(4 dpf *biluo*)=5 embryos, n(7 dpf sibling)=4 embryos, n(7 dpf *biluo*)=5 embryos. **P<0.01 Error bars represent mean ± SD.

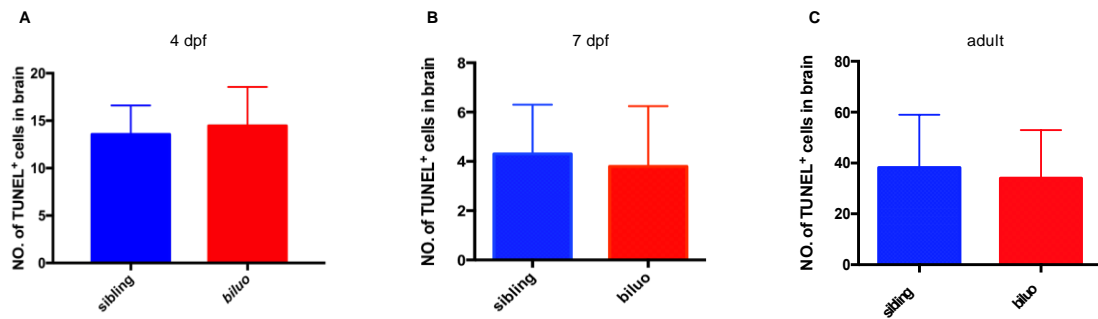


Figure S3 related to Figure 3. **Terminal Deoxynucleotidyl Transferase dUTP Nick End Labeling (TUNEL) Staining in Embryonic and Adult Brains of *biluo* Mutants.**

(A) Quantification data of the number of TUNEL positive cells in 4 dpf mid-brain in siblings (blue) and *biluo* mutants (red). n(sibling)=9 embryos, n(*biluo*)=11 embryos, p=0.765. Error bars represent mean \pm SD.

(B) Quantification data of the number of TUNEL positive cells in 7 dpf mid-brain in siblings (blue) and *biluo* mutants (red). n(sibling)=10 embryos, n(*biluo*)=10 embryos, p=0.623. Error bars represent mean \pm SD.

(C) Quantification data of the number of TUNEL positive cells in adult brain in siblings (blue) and *biluo* mutants (red). n(sibling)=4 fish, n(*biluo*)=4 fish, p=0.7726. Error bars represent mean \pm SD.

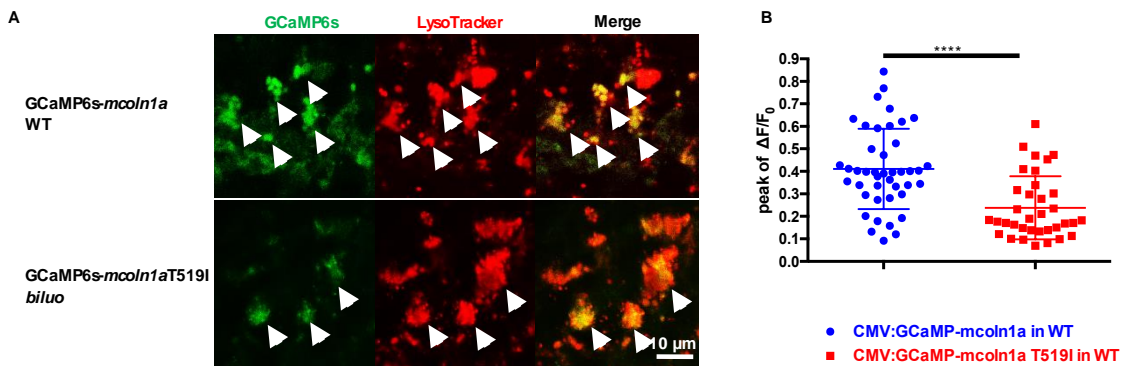


Figure S4 related to Figure 4. **Co-localization of WT and Mutant GCaMP6s-mcoln1a with LysoTracker.**

(A) Anti-GFP and LysoTracker double staining shows co-localization of LysoTracker with WT (GCaMP6s-*mcoln1a*) and mutant (GCaMP6s-*mcoln1a* T519I) proteins in WT and *biluo* embryos injected with the WT GCaMP6s-*mcoln1a* and mutant GCaMP6s-*mcoln1a*T519I constructs respectively. White arrows indicate the co-localization.

(B) Quantification of the mean of the peak of $\Delta F/F_0$ (representing Trpm1a-mediated Ca^+ efflux) in the macrophages in WT embryos injected with WT CMV:GCaMP6s-*trpm1a* construct (blue dots) and mutant CMV:GCaMP6s-*trpm1a* T519I (red square). $\Delta F/F_0$ is calculated as $(F-F_0)/F_0$, where F_0 is the baseline fluorescence signal. **** P < 0.0001, Error bars represent mean±SD. n(WT late endosome)=43, n(*biluo* late endosome)=35

3 dpf, *mcoln1a* expression, FITC

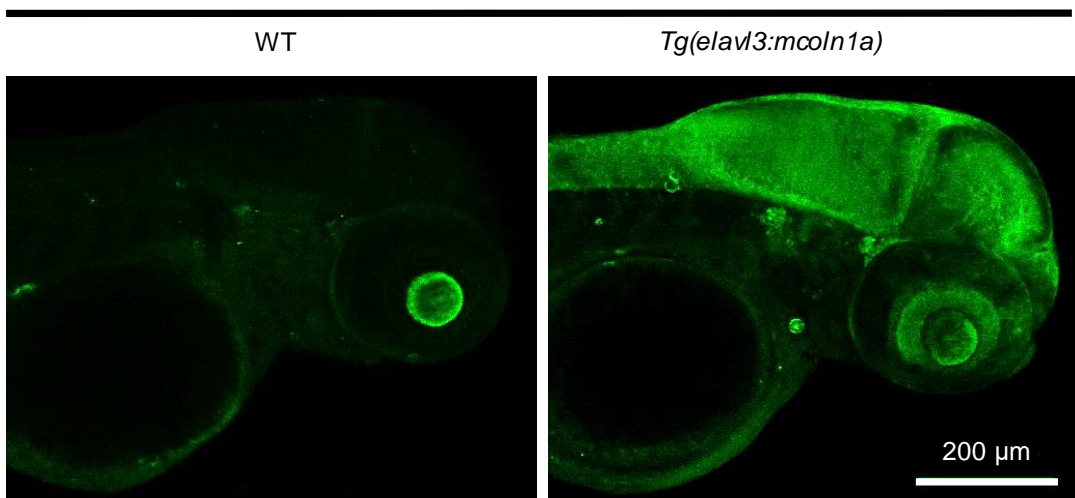


Figure S5 related to Figure 5. **The Expression of *mcoln1a* in *Tg(elavl3:mcoln1a)*.**

In-situ hybridization indicates *mcoln1a* expression in *Tg(elavl3:mcoln1a)* and WT embryos at 3 dpf.

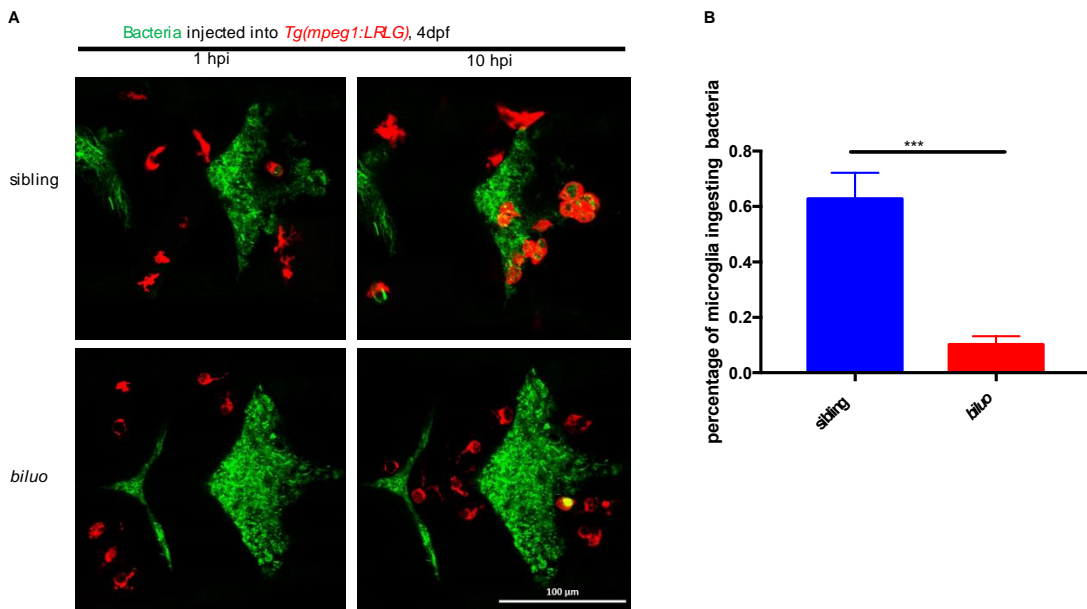


Figure S6 related to Figure 5. **Microglia in *biluo* Mutants Have Decreased Engulfment Ability.**

(A) GFP bacteria was injected into the brain of sibling (upper panels) and *biluo* mutants (lower panels) at 4 dpf and images were taken at 1 hpi (left panels) and 10 hpi (right panels).

(B) Quantification of the percentage of microglia engulfing green bacteria at 10 hpi. n(sibling)=4, n(*biluo*)=4. ***P<0.001, t-test. Error bars represent mean \pm SD.

TRANSPARENT METHODS

Zebrafish

Zebrafish were raised and maintained as described (Westerfield). AB, WIK strain, *biluo*^{hkz12}, *Tg(coro1a:GFP)* (Li et al., 2012a), *Tg(hsp70:mCherry-T2a-CreERT2) #12* (Hans et al., 2011), *Tg(mpeg1:loxP-DsRedx-loxP-GFP)hkz15Tg* (Xu et al., 2015), *Tg(elavl3:GCaMP6s)* (Cong et al., 2017), *Tg(coro1a:mcoln1a)hkz20Tg* and *Tg(elavl3:mcoln1a)hkz21Tg* were used in this study. All experiments were conducted with approval of the Animal Ethics Committee of the Hong Kong University of Science and Technology.

Ethylnitrosourea (ENU) Mutagenesis and Neutral Red Staining

ENU (Sigma, USA) mutagenesis was carried out as described (Mullins et al., 1994; Solnica-Krezel et al., 1994). Neutral red staining was performed as reported (Herbomel et al., 2001).

Positional Cloning

Positional cloning was performed as described previously (Bahary et al., 2004). Bulk two simple sequence length polymorphism markers (SSLPs) markers zC214C7I and 211668r. Sequencing of candidate genes within the region revealed a C to T mutation in the *mcoln1a* gene.

Generation of Transgenic Lines

The coding regions of the *mcoln1a* gene was placed under the control of the *elavl3* and *coro1a* promoters and inserted into the pTol2 vector. The generation of transgenic fish lines were performed as described (Kawakami et al., 2000).

Whole-Mount *in situ* Hybridization (WISH)

Antisense DIG labeled RNA probes of *mcoln1a* was synthesized *in vitro*. WISH was carried out according to the standard protocol (Westerfield).

Whole-Mount Antibody Staining

Whole-mount antibody staining was performed as described (Barresi et al., 2000; Jin

et al., 2009). The primary antibodies used in this study are: Anti-GFP antibody (ab6658, Abcam; 1:800 dilution), Anti-LAMP1 antibody (ab24170, Abcam; 1:800 dilution), Anti-Lcp1 antibody (1:400 dilution) (Jin et al., 2009) and Anti-Mcoln1a antibody (1:400 dilution). The secondary antibodies used are: Alexa 488-anti-goat antibody (A11055 Invitrogen), Alexa 555-anti-rabbit antibody (A31572 Invitrogen) and Alexa 647-anti-rabbit antibody (A31573 Invitrogen). Images were captured by Leica SP8 confocal microscope.

Terminal Deoxynucleotidyl Transferase dUTP Nick End Labeling (TUNEL) Staining

TUNEL staining was performed using the *In Situ* Cell Death Detection Kit TMR red (Roche) according to the manufacturer's instructions.

Lysotracker Staining

Embryos were maintained in egg water containing PTU (1-phenyl 2-thiourea) and incubated with Lysotracker™ Red DND-99 (Invitrogen™) at 50 nM for 10 minutes. After washing with egg water for three times, the embryos were imaged by Leica SP8 confocal microscope. Microglia in the optic tectum of brain were imaged, whereas peripheral macrophages in the CHT region were imaged.

Calcium Release Assay

We injected CMV:GCaMP6s-*mcoln1a* or CMV:GCaMP6s-*mcoln1a*T519I into WT or *biluo* mutant embryos. Around 2 dpf, before microglia precursors entering into brain, we performed *in vivo* live imaging to record calcium release of Mcoln1a channel in peripheral macrophages in the CHT region. Individual late endosomes or lysosomes were manually segmented on the average image after registration by MultiStackReg plugin in ImageJ. De-trend and noise reduction were performed by a self-written MATLAB program. Calcium events were detected as peaks by a self-written MATLAB program. For each late endosome or lysosome, we averaged the amplitude of calcium peak as its amplitude of calcium release during the recording time.

Single Microglia Collection and Genotyping

In this experiment, three types of 3 dpf embryos, *Tg(mpeg1:LRLG)*, *biluo;Tg(mpeg1-LRLG)* and *biluo;Tg(mpeg1-LRLG;corola:mcoln1a)*, were used. In each group, the brains of 15 embryos with strong red fluorescence were dissected and dissociated by Dispase (Roche) to single cell solution. Then single *mpeg1*⁺ cells (microglia) with intact morphology under fluorescent microscope was picked manually and immediately suspended in lysis buffer. Two single cells were pulled together to generate cDNA libraries using Smart-seq2 method (Picelli et al., 2014). Primers used for genotyping are:

FP-CTGTTGCTGTGGCGGTGATCT, RP-
GTTGACAAGGAGGACGTCCCTCA.

WT *mcoln1a* but not mutant *mcoln1aT519I* PCR products can be digested by MspI into two 200 bp fragments.

In vivo Confocal Calcium Imaging

Larval zebrafish (6 dpf) were embedded in 1.5% low-melting agarose after paralysis by 0.1% α -bungarotoxin. Calcium images were taken by an Olympus Fluoview 1000 upright confocal microscope (Tokyo, Japan) with a 40 \times water-immersion objective (NA = 0.80). Frames with an approximate 150 \times 150 μm^2 field of view of one-side optic tectum (about 350 \times 350 pixel² and 0.397 \times 0.397 μm^2 per pixel) were acquired at about 1.2 Hz. Individual neurons were manually segmented on the average image after registration by MultiStackReg plugin in ImageJ. De-trend and noise reduction were performed by a self-written MATLAB program. Fluorescence lower than 10 % (threshold) was reassigned zero. Calcium events were detected as peaks by a self-written MATLAB program. For visual responses, a true positive response was identified if the maximal fluorescence after stimulation is larger than \pm 2 SD of the baseline.

Visual Stimulation

Light flashes were generated by a red LED to avoid the interference of spectrum to cesium imaging. The LED and imaging setup were coupled by Master 8. Visual stimuli included 5 trials and each flash lasted for 2 second with 60 s interval. Visual stimuli were shed on one-side of eye and calcium images were taken on the contralateral optic tectum according to retinotopic maps.

Statistical Analysis

F-test was performed to test two sample variances. According to the results of F-test, two-sample T-test was performed assuming equal or unequal variances. Statistical analysis was performed by Data Analysis tool of Excel software (Microsoft). Two-tailed P values were used in all T tests. To make multi-group comparison, one-way ANOVA was performed followed by Tukey's multiple comparisons test. ANOVA analysis was performed by GraphPad software. In calcium imaging experiment, Kolmogorov-Smirnov test was applied in Matlab.

SUPPLEMENTAL REFERENCES

Bahary, N., Davidson, A., Ransom, D., Shepard, J., Stern, H., Trede, N., Zhou, Y., Barut, B., and Zon, L.I. (2004). The Zon laboratory guide to positional cloning in zebrafish. Methods in cell biology 77, 305-329.

Barresi, M.J., Stickney, H.L., and Devoto, S.H. (2000). The zebrafish slow-muscle-omitted gene product is required for Hedgehog signal transduction and the development of slow muscle identity. Development 127, 2189-2199.

Cong, L., Wang, Z., Chai, Y., Hang, W., Shang, C., Yang, W., Bai, L., Du, J., Wang, K., and Wen, Q. (2017). Rapid whole brain imaging of neural activity in freely behaving larval zebrafish (*Danio rerio*). eLife 6.

Hans, S., Freudenreich, D., Geffarth, M., Kaslin, J., Machate, A., and Brand, M. (2011). Generation of a non-leaky heat shock-inducible Cre line for conditional Cre/lox strategies in zebrafish. Developmental dynamics: an official publication of the American Association of Anatomists 240, 108-115.

Jin, H., Sood, R., Xu, J., Zhen, F., English, M.A., Liu, P.P., and Wen, Z. (2009). Definitive hematopoietic stem/progenitor cells manifest distinct differentiation output in the zebrafish VDA and PBI. Development 136, 647-654.

Kawakami, K., Shima, A., and Kawakami, N. (2000). Identification of a functional transposase of the Tol2 element, an Ac-like element from the Japanese medaka fish, and its transposition in the zebrafish germ lineage. Proc Natl Acad Sci U S A 97, 11403-11408.

Li, L., Yan, B., Shi, Y.Q., Zhang, W.Q., and Wen, Z.L. (2012a). Live imaging reveals differing roles of macrophages and neutrophils during zebrafish tail fin regeneration. The Journal of biological chemistry 287, 25353-25360.

Mullins, M.C., Hammerschmidt, M., Haffter, P., and Nusslein-Volhard, C. (1994). Large-scale mutagenesis in the zebrafish: in search of genes controlling development in a vertebrate. Current biology: CB 4, 189-202.

Picelli S, Faridani O R, Björklund A K, et al. Full-length RNA-seq from single cells using Smart-seq2.[J]. Nature Protocols, 2014, 9(1):171-181.

Solnica-Krezel, L., Schier, A.F., and Driever, W. (1994). Efficient recovery of ENU-induced mutations from the zebrafish germline. Genetics 136, 1401-1420.

Westerfield, M. *The zebrafish book: A Guide for the Laboratory Use of Zebrafish (Danio rerio)* 3rd ed (Eugene, OR: University of Oregon Press, 1995).

Xu, J., Zhu, L., He, S., Wu, Y., Jin, W., Yu, T., Qu, J.Y., and Wen, Z. (2015). Temporal-Spatial Resolution Fate Mapping Reveals Distinct Origins for Embryonic and Adult Microglia in Zebrafish. Developmental cell 34, 632-641.